Hindawi
Mathematical Problems in Engineering
Volume 2019, Article ID 2697242, 10 pages
https://doi.org/10.1155/2019/2697242

*Research Article*

# Numerical and Experimental Analysis of the Dynamic Behavior of Piezoelectric Stiffened Composite Plates Subjected to Airflow

**Nguyen Thai Chung**,[1] **Nguyen Ngoc Thuy**,[1] **Duong Thi Ngoc Thu**,[2] **and Le Hai Chau**[1]

[1]*Department of Solid Mechanics, Le Quy Don Technical University, Hanoi, Vietnam*
[2]*University of Transport Technology, Hanoi, Vietnam*

Correspondence should be addressed to Nguyen Thai Chung; chungnt@mta.edu.vn

Received 1 October 2018; Accepted 2 December 2018; Published 29 January 2019

Academic Editor: Giuseppe Vairo



In this paper, the authors present results on dynamic behavior analysis of the stiffened composite plate with piezoelectric patches under airflow by finite element method and experimental study. The first-order shear deformation plate theory and nine-noded isoparametric piezoelectric laminated plate finite element with five elastic degrees of freedom at each node and one electric degree of freedom per element per piezoelectric layer were used in the dynamic analysis of plates by finite element method. The modern equipment was used in the dynamic behaviors analysis of plates subjected to airflow load by experimental method. In this study, the results of the theoretical method have been compared with experimental studies.

## 1. Introduction

The research and development of smart stiffened composite structures represent one of the most significant recent trends in the mechanics of structures, especially in the aerospace industry. These structures can provide significant advantages over traditional structures, notably active vibration control. In 1957 and 1959, the first investigations of piezoelectric structures were published by Haskins and Walsh [1] and Toupin [2] who considered cylindrical and spherical shells, respectively. Tiersten's [3] analysis was in linear vibrations of piezoelectric plates. Adelman and Stavsky [4] studied vibrations of composite cylinders by piezoceramic and metallic layers. V. Balamurugan, S. Narayanon and Rajan L.Wankhade, Kamal M.B [5, 6] studied consistency technique for vibration control of smart stiffened plates using distributed piezoelectric sensors and actuators subjected to cyclic loads. P.veera Sanjeeva Kumar, B.Chandra Mohana Reddy [7] have presented a paper on the vibration of smart composite laminate plates using higher order theory. Sangamesh B. Herakal, Sai Kumar Dathrika, P. Giriraj Goud, and P. Sravan [8] analyzed bending of the smart composite plate under thermal environment, and Kanjuro Makihara, Junjiro Onoda, and Kenji Minesugi [9] studied flutter of cantilevered plate wing with piezoelectric material layers by finite element method. In 2016, Zafer K and Zahit M [10] presented a paper on flutter analysis of a laminated composite plate with temperature dependent material properties. N. T. Chung, H. X. Luong, and N. T. T. Xuan [11] studied the dynamic stability of laminated composite plate with piezoelectric layers. N. N. Thuy and N. T. Chung [12] have presented a paper on the dynamic analysis of smart stiffened composite plates using higher order theory.

In this paper, in order to have more studies about the dynamic responses of piezoelectric composite plates, the authors examine the problems with piezoelectric stiffened composite plates subjected to airflow by finite element and experimental method.

## 2. Finite Element Formulation and the Governing Equations

Consider isoparametric piezoelectric laminated stiffened plate with the general coordinate system (x, y, z), in which the x, y plane coincides with the neutral plane of the plate. The top surface and lower surface of the plate are bonded to the piezoelectric patches (actuator and sensor). The plate is subjected to the airflow load acting (Figure 1).

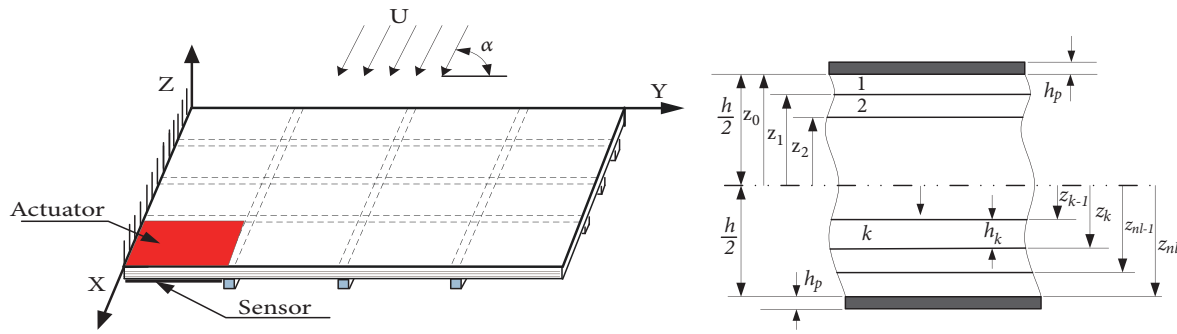


Figure 1: Smart stiffened plate and coordinate system (a), and lamina details (b).

*2.1. Piezoelectric Equations.* Consider a laminated composite plate with integrated sensors and actuators as shown in Figure 1. It is assumed that each layer of the plate possesses a plane of elastic symmetry parallel to the x-y plane; the $k^{th}$ layer's lamina constitutive equations coupling the direct and converse piezoelectric equations can be expressed as [13, 14]

$$\begin{Bmatrix}\sigma_1\\ \sigma_2\\ \tau_{12}\end{Bmatrix}_k = \begin{bmatrix}\overline{Q}_{11} & \overline{Q}_{12} & 0\\ \overline{Q}_{12} & \overline{Q}_{22} & 0\\ 0 & 0 & \overline{Q}_{66}\end{bmatrix}_k \begin{Bmatrix}\varepsilon_1\\ \varepsilon_2\\ \gamma_{12}\end{Bmatrix}_k - \begin{bmatrix}0 & 0 & \overline{e}_{31}\\ 0 & 0 & \overline{e}_{32}\\ 0 & 0 & 0\end{bmatrix}_k \begin{Bmatrix}E_1\\ E_2\\ E_3\end{Bmatrix}_k, \tag{1}$$

$$\begin{Bmatrix}D_1\\ D_2\\ D_3\end{Bmatrix}_k = \begin{bmatrix}0 & 0 & 0\\ 0 & 0 & 0\\ \overline{e}_{31} & \overline{e}_{32} & 0\end{bmatrix}_k \begin{Bmatrix}\varepsilon_1\\ \varepsilon_2\\ \gamma_{12}\end{Bmatrix}_k + \begin{bmatrix}\overline{p}_{11} & 0 & 0\\ 0 & \overline{p}_{22} & 0\\ 0 & 0 & \overline{p}_{33}\end{bmatrix}_k \begin{Bmatrix}E_1\\ E_2\\ E_3\end{Bmatrix}_k, \tag{2}$$

where $\overline{Q}_{ij}$, $\overline{e}_{ij}$, $\overline{p}_{ij}$ are, respectively, the plane-stress reduced elastic constants, the piezoelectric constants, and the permittivity coefficients of the $k^{th}$ lamina in its material coordinate system; $\{\sigma\}_k = \{\sigma_1\ \sigma_2\ \tau_{12}\}_k^T$, $\{\varepsilon\}_k = \{\varepsilon_1\ \varepsilon_2\ \gamma_{12}\}_k^T$, $\{E\}_k = \{E_1\ E_2\ E_3\}_k^T$, $\{D\}_k = \{D_1\ D_2\ D_3\}_k^T$ are the stress, strain, electric field, and electric displacement matric components, respectively, to the material coordinate system. If the voltage is applied to the actuator in the thickness only, then $\{E\}_k = \{0\ 0\ -1/h_k\}^T \phi_k = [B_\phi]\phi_k$, $V_k$ is the applied voltage across the $k^{th}$ ply, and $h_k$ is the thickness of the $k^{th}$ piezoelectric layer. The plane-stress reduced elastic constants $\overline{Q}_{ij}$ are given as

$$\begin{aligned}\overline{Q}_{11} &= \frac{E_1}{1-\nu_{12}\nu_{21}},\\ \overline{Q}_{12} &= \frac{\nu_{12}E_2}{1-\nu_{12}\nu_{21}},\\ \overline{Q}_{22} &= \frac{E_2}{1-\nu_{12}\nu_{21}},\\ \overline{Q}_{66} &= G_{12},\end{aligned} \tag{3}$$

Upon transformation, the lamina piezoelectric equations can be expressed in terms of the stress, strains, and electric displacements in the plate coordinates as [13, 14]

$$\begin{Bmatrix}\sigma_x\\ \sigma_y\\ \tau_{xy}\end{Bmatrix}_k = \begin{bmatrix}Q_{11} & Q_{12} & Q_{16}\\ Q_{12} & Q_{22} & Q_{26}\\ Q_{16} & Q_{26} & Q_{66}\end{bmatrix}_k \begin{Bmatrix}\varepsilon_x\\ \varepsilon_y\\ \gamma_{xy}\end{Bmatrix}_k - \begin{bmatrix}0 & 0 & e_{31}\\ 0 & 0 & e_{32}\\ 0 & 0 & e_{36}\end{bmatrix}_k \begin{Bmatrix}E_x\\ E_y\\ E_z\end{Bmatrix}_k, \tag{4}$$

$$\begin{Bmatrix}D_x\\ D_y\\ D_z\end{Bmatrix}_k = \begin{bmatrix}0 & 0 & 0\\ 0 & 0 & 0\\ e_{31} & e_{32} & e_{36}\end{bmatrix}_k \begin{Bmatrix}\varepsilon_x\\ \varepsilon_y\\ \gamma_{xy}\end{Bmatrix}_k + \begin{bmatrix}p_{11} & p_{12} & 0\\ p_{12} & p_{22} & 0\\ 0 & 0 & p_{33}\end{bmatrix}_k \begin{Bmatrix}E_x\\ E_y\\ E_z\end{Bmatrix}_k. \tag{5}$$

Equations (4) and (5) can also be written as

$$\{\sigma\}_k = [Q]_k\{\varepsilon\}_k - [e]_k^T\{E\}_k, \tag{6}$$

$$\{D\}_k = [e]_k\{\varepsilon\}_k + [p]_k\{E\}_k, \tag{7}$$

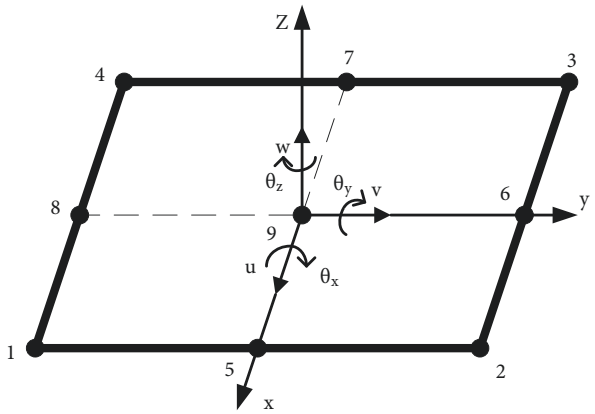


Figure 2: Smart piezoelectric composite plate element.

The $Q_{ij}$ are the components of the transformed lamina stiffness matrix which are defined as follows:

$$\begin{aligned}
Q_{11} &= \overline{Q}_{11}\cos^4\theta + \overline{Q}_{22}\sin^4\theta \\
&\quad + 2\left(\overline{Q}_{12} + 2\overline{Q}_{66}\right)\sin^2\theta\cos^2\theta, \\
Q_{12} &= \left(\overline{Q}_{11} + \overline{Q}_{22} - 4\overline{Q}_{66}\right)\sin^2\theta\cos^2\theta \\
&\quad + \overline{Q}_{12}\left(\sin^4\theta + \cos^4\theta\right), \\
Q_{22} &= \overline{Q}_{11}\sin^4\theta + \overline{Q}_{22}\cos^4\theta \\
&\quad + 2\left(\overline{Q}_{12} + 2\overline{Q}_{66}\right)\sin^2\theta\cos^2\theta, \\
Q_{16} &= \left(\overline{Q}_{11} - \overline{Q}_{12} - 2\overline{Q}_{66}\right)\cos^3\theta\sin\theta \\
&\quad - \left(\overline{Q}_{22} - \overline{Q}_{12} - 2\overline{Q}_{66}\right)\sin^3\theta\cos\theta, \\
Q_{26} &= \left(\overline{Q}_{11} - \overline{Q}_{12} - 2\overline{Q}_{66}\right)\sin^3\theta\cos\theta \\
&\quad - \left(\overline{Q}_{22} - \overline{Q}_{12} - 2\overline{Q}_{66}\right)\sin\theta\cos^3\theta, \\
Q_{66} &= \left(\overline{Q}_{11} + \overline{Q}_{12} - 2\overline{Q}_{12} - 2\overline{Q}_{66}\right)\sin^2\theta\cos^2\theta \\
&\quad + \overline{Q}_{66}\left(\sin^4\theta + \cos^4\theta\right),
\end{aligned} \tag{8}$$

where $\theta$ is the lamina orientation angle.

The piezoelectric constants matrix [e] is unavailable and it can be expressed by the more commonly available piezoelectric strain constant matrix which is [d] as [13]

$$[e] = [d][Q], \tag{9}$$

where $[d] = \begin{bmatrix} 0 & 0 & 0 & d_{15} & 0 \\ 0 & 0 & d_{24} & 0 & 0 \\ d_{31} & d_{32} & 0 & 0 & 0 \end{bmatrix}$.

*2.2. Smart Piezoelectric Composite Plate Element Formulation.* A smart piezoelectric composite plate element is considered with coordinates x, y along the in-plane direction and z along the thickness direction as shown in Figure 2.

Using the Mindlin formulation, the displacements u, v, and w at a point (x,y,z) form the median surface and are expressed as functions of mid-plane displacements $u_0$, $v_0$, and $w_0$ and independent rotations $\theta_x$ and $\theta_y$ of the normal in xz and yz planes, respectively, as [11, 15, 16]

$$\begin{aligned}
u(x,y,z,t) &= u_0(x,y,t) + z\theta_y(x,y,t), \\
v(x,y,z,t) &= v_0(x,y,t) - z\theta_x(x,y,t), \\
w(x,y,z,t) &= w_0(x,y,t),
\end{aligned} \tag{10}$$

The components of the strain vector corresponding to the displacement field (10) are [7, 11]

$$\begin{Bmatrix} \varepsilon_x \\ \varepsilon_y \\ \gamma_{xy} \end{Bmatrix} = \left\{\varepsilon_b^{ln}\right\} + \left\{\varepsilon^{nl}\right\} = \left\{\varepsilon_b\right\}, \tag{11}$$

where $\{\varepsilon_b^{ln}\}$, $\{\varepsilon_b^{nl}\}$ are the linear and nonlinear strain vector, respectively, and defined as follows:

$$\begin{aligned}
\left\{\varepsilon_b^{ln}\right\} &= \begin{Bmatrix} \varepsilon_x \\ \varepsilon_y \\ \gamma_{xy} \end{Bmatrix} = \begin{Bmatrix} \varepsilon_x^o \\ \varepsilon_y^o \\ \gamma_{xy}^o \end{Bmatrix} + z\begin{Bmatrix} \kappa_x \\ \kappa_y \\ \kappa_{xy} \end{Bmatrix} \\
&= \begin{bmatrix} \dfrac{\partial}{\partial x} & 0 \\ 0 & \dfrac{\partial}{\partial y} \\ \dfrac{\partial}{\partial y} & \dfrac{\partial}{\partial x} \end{bmatrix}\begin{Bmatrix} u_0 \\ v_0 \end{Bmatrix} + z\begin{bmatrix} -\dfrac{\partial}{\partial y} & 0 \\ 0 & -\dfrac{\partial}{\partial x} \\ -\dfrac{\partial}{\partial y} & \dfrac{\partial}{\partial x} \end{bmatrix}\begin{Bmatrix} \theta_x \\ \theta_y \end{Bmatrix} \\
&= \left\{\varepsilon_0\right\} + z\left\{\kappa\right\}, \\
\left\{\varepsilon_b^{nl}\right\} &= \frac{1}{2}\begin{bmatrix} \dfrac{\partial w_0}{\partial x} & 0 \\ 0 & \dfrac{\partial w_0}{\partial y} \\ \dfrac{\partial w_0}{\partial y} & \dfrac{\partial w_0}{\partial x} \end{bmatrix}\begin{Bmatrix} \dfrac{\partial}{\partial x} \\ \dfrac{\partial}{\partial y} \end{Bmatrix} w_0.
\end{aligned} \tag{12}$$

In the finite formulation, the displacement field {u} and the electric potential $\{\phi\}$ over an element are related to the corresponding node values $\{u\}_e$ of the element and the electric charges of the piezo layer $\{\phi\}_e$ by the mean of the shape functions $[N_u]$, $[N_\phi]$, as follows [15]:

$$\{u\} = [N_u]\{q\}_e, \tag{13}$$

$$\{\phi\} = [N_\phi]\{\phi\}_e. \tag{14}$$

Equation (11) can be expressed as

$$\{\varepsilon\} = \left[B_u^{ln}\right]\{u\}_e + \left[B_u^{nl}\right]\{u\}_e. \tag{15}$$

where $[B_u^{ln}]$ and $[B_u^{nl}]$ are linear and nonlinear strain matric, respectively, $[N_u]$ are the shape functions, and $[N_\phi]$ are the shape functions for the electric potential.

The dynamic equations of a finite smart laminated composite plate can be derived by using Hamilton's principle [15, 17]:

$$\delta \int_{t_1}^{t_2} \left(T^e - U^e + W^e\right) dt = 0, \tag{16}$$

where $T^e$ is the kinetic energy, $U^e$ is the strain energy, and $W^e$ is the work done by the applied forces.

The kinetic energy at the element level is defined as

$$T^e = \frac{1}{2} \int_{V_e} \rho \{\dot{u}\}^T \{\dot{u}\} \, dV, \tag{17}$$

where $V_e$ is the volume of the plate element.

The strain energy can be written as

$$U^e = \frac{1}{2} \int_{V_e} \{\varepsilon\}^T \{\sigma\} \, dV, \tag{18}$$

The work done by the external forces

$$W^e = \int_{V_e} \{u\}^T \{f_b\} \, dV + \int_{S_e} \{u\}^T \{f_s\} \, dS + \{u\}^T \{f_c\}, \tag{19}$$

where $\{f_b\}$ is the body force, $S_e$ is the surface area of the plate element, $\{f_s\}$ is the surface force, and $\{f_c\}$ is the concentrated load.

Substituting (17), (18), and (19) into (16), noting that the electric field vector $\{E\} = -[B_\phi]\{\phi\}_e$, and using (6), (7), (13), (14), and (15), the dynamic matrix equations can be written as

$$\begin{aligned} &[M]_e \{\ddot{u}\}_e + \left(\left[K_{uu}^{ln}\right]_e + \left[K_{uu}^{nl}\right]_e\right)\{u\}_e + \left[K_{u\phi}\right]_e \{\phi\}_e \\ &\quad = \{f\}_e^m, \end{aligned} \tag{20}$$

$$\left[K_{\phi u}\right]_e \{u\}_e + \left[K_{\phi\phi}\right]_e \{\phi\}_e = \{\Phi\}_e^{pz}, \tag{21}$$

Substitute (21) into (20) to obtain

$$\begin{aligned} &[M]_e \{\ddot{u}\}_e \\ &\quad + \left(\left[K_{uu}^{ln}\right]_e + \left[K_{uu}^{nl}\right]_e - \left[K_{u\phi}\right]_e \left[K_{\phi\phi}\right]_e^{-1} \left[K_{\phi u}\right]_e\right)\{u\}_e \\ &\quad = \{f\}_e^m - \left[K_{u\phi}\right]_e \left[K_{\phi\phi}\right]_e^{-1} \{\Phi\}_e^{pz}, \end{aligned} \tag{22}$$

where $[M]_e = \int_{V_e} \rho [N_u]^T [N_u] dV$, $[K_{uu}^{ln}]_e = \int_{V_e} [B_u^{ln}]^T [Q] [B_u^{ln}] dV$, $[K_{uu}^{nl}]_e = \int_{V_e} [B_{uu}^{nl}]^T [Q] [B_{uu}^{nl}] dV$, $[K_{u\phi}]_e = \int_{V_e} [B_u]^T [e]^T [B_\phi] dV$, $[K_{\phi\phi}]_e = \int_{V_e} [B_\phi]^T [p] [B_\phi] dV$, $[K_{\phi u}]_e = [K_{u\phi}]_e^T$, which are, respectively, the element mass, linear mechanical stiffness, nonlinear mechanical stiffness, mechanical-electrical coupling, piezoelectric permittivity, and electrical-mechanical coupling matrix. The vector $\{f\}_e^m$ and $\{\Phi\}_e^{pz}$ are element external mechanical force vector and external voltage applied to the piezo layer, respectively, which are defined as follows:

$$\begin{aligned} \{f\}_e^m = &\int_{V_e} [N_u]^T \{f_b\} \, dV + \int_{S_e} [N_u]^T \{f_s\} \, dS \\ &+ [N_u]^T \{f_c\}, \end{aligned} \tag{23}$$

For the sensor layer, charge sensing is considered. With zero voltage, from (21), the sensed voltage $\{\phi^s\}_e$ is given by [13, 16, 18]

$$\{\phi^s\}_e = -\left[K_{\phi\phi}^s\right]_e^{-1} \left[K_{\phi u}^s\right]_e \{u\}_e. \tag{24}$$

The operation of the amplified control loop implies the actuating voltage is

$$\{\phi^a\}_e = G_d \{\phi^s\}_e + G_v \left\{\dot{\phi}^s\right\}_e, \tag{25}$$

where $G_d$ and $G_v$ are the feedback control gains for displacement and velocity, respectively.

From (21), the charge in the actuator due to actuator strain in response to plate vibration modified by control system feedback is

$$\begin{aligned} \{\Phi^a\}_e &= \left[K_{\phi u}\right]_e \{u\}_e + \left[K_{\phi\phi}\right]_e \left(G_d \{\phi^s\}_e + G_v \left\{\dot{\phi}^s\right\}_e\right) \\ &= \left[K_{\phi u}\right]_e \{u\}_e - G_d \left[K_{\phi\phi}\right]_e \left[K_{\phi\phi}^s\right]_e^{-1} \left[K_{\phi u}^s\right]_e \{u\}_e \\ &\quad - G_v \left[K_{\phi\phi}\right]_e \left[K_{\phi\phi}^s\right]_e^{-1} \left[K_{\phi u}^s\right]_e \{\dot{u}\}_e. \end{aligned} \tag{26}$$

Substitute (26) into (22) to yield

$$\begin{aligned} &[M]_e \{\ddot{u}\}_e - G_v \left[K_{u\phi}\right]_e \left[K_{\phi\phi}\right]_e^{-1} \left[K_{\phi\phi}\right]_e \left[K_{\phi\phi}^s\right]_e^{-1} \left[K_{\phi u}^s\right]_e \\ &\quad \cdot \{\dot{u}\}_e + \left(\left[K_{uu}^{ln}\right]_e + \left[K_{uu}^{nl}\right]_e \right. \\ &\quad \left. - G_d \left[K_{u\phi}\right]_e \left[K_{\phi\phi}\right]_e^{-1} \left[K_{\phi\phi}\right]_e \left[K_{\phi\phi}^s\right]_e^{-1} \left[K_{\phi u}^s\right]_e\right)\{u\}_e \\ &\quad = \{f\}_e^m, \end{aligned} \tag{27}$$

where $[K_{\phi u}^s]_e = [K_{\phi u}^a]_e = [K_{\phi u}]_e$ and $[K_{\phi\phi}^s]_e = [K_{\phi\phi}^a]_e = [K_{\phi\phi}]_e$ are the mechanical-electrical coupling and pizoelectric permittivity stiffness matrices, respectively.

Equation (27) can be rewritten as follows:

$$\begin{aligned} &[M]_e \{\ddot{u}\}_e + \left[C_A\right]_e \{\dot{u}\}_e \\ &\quad + \left(\left[K_{uu}^{ln}\right]_e + \left[K_{uu}^{nl}\right]_e + \left[K_A\right]_e\right)\{u\}_e = \{f\}_e^m, \end{aligned} \tag{28}$$

where $[C_A]_e = -G_v [K_{u\phi}]_e [K_{\phi\phi}]_e^{-1} [K_{\phi\phi}]_e [K_{\phi\phi}^s]_e^{-1} [K_{\phi u}^s]_e$ is the element active damping matrix and $[K_A]_e = -G_d [K_{u\phi}]_e [K_{\phi\phi}]_e^{-1} [K_{\phi\phi}]_e [K_{\phi\phi}^s]_e^{-1} [K_{\phi u}^s]_e$ is the element active stiffness matrix.

### 2.3. Formulation of Stiffener

#### 2.3.1. Formulation of x-Stiffener

$$\begin{aligned} U_{xs}(x, z) &= u_0(x) + z\theta_{xs}(x), \\ W_{xs}(x, z) &= w_{xs}(x), \end{aligned} \tag{29}$$

where x-axis is taken along the stiffener centerline and the z-axis is its upward normal. The plate and stiffener element are shown in Figure 3.

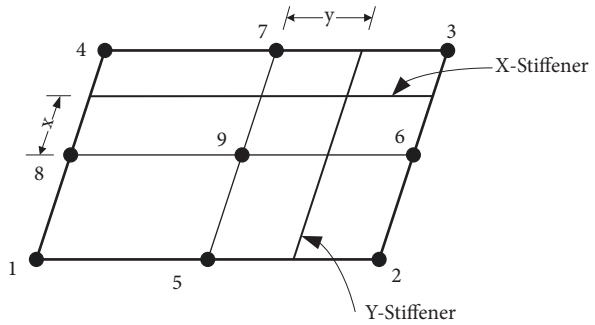


Figure 3: Modeling of plate and stiffener element.

If we consider that the x-stiffener is attached to the lower side of the plate, conditions of displacement compatibility along their line of connection can be written as

$$\begin{aligned} u_p\big|_{z=-t_p/2} &= u_{xs}\big|_{z=t_{xs}/2}, \\ \theta_{xp}\big|_{z=-t_p/2} &= \theta_{xs}\big|_{z=t_{xs}/2}, \\ w_p\big|_{z=-t_p/2} &= w_{xs}\big|_{z=t_{xs}/2}, \end{aligned} \tag{30}$$

where $t_p$ is the plate thickness and $t_{xs}$ is the x-stiffener depth.

The element stiffness and mass matrices are defined as follows [15]:

$$\left[K_{xs}\right]_e = \int_{l_e} \left[B_{xs}\right]^T \left[D_{xs}\right] \left[B_{xs}\right] dx, \tag{31}$$

$$\begin{aligned} \left[M_{xs}\right]_e = \int_{A_e} \Big[ & P\left(\left[N_{u^0}\right]^T \left[N_{u^0}\right] + \left[N_w\right]^T \left[N_w\right]\right) \\ & + I_y \left(\left[N_{\theta_x}\right]^T \left[N_{\theta_x}\right]\right)\Big] dA, \end{aligned} \tag{32}$$

where $[B_{xs}]$ is the strain-displacement relations matrix, $[D_{xs}]$ is the stress-strain relations matrix, and $l_e$ is the element length. $[N_{u^0}]$, $[N_w]$ and $[N_{\theta_x}]$ are the shape function matrices relating the primary variables $u_0$, w, x, in terms of nodal unknowns, $I_y$ is the area moment of inertia related to the y-axis, and $P = \sum_{k=1}^{n} \int_{h_{k-1}}^{h_k} \rho_k dz$, with $\rho_k$ being density of $k^{th}$ layer.

*2.3.2. Formulation of y-Stiffener.* The same as for x-stiffener, the element stiffness and mass matrices of the y-stiffener are defined as follows:

$$\left[K_{ys}\right]_e = \int_{l_e} \left[B_{ys}\right]^T \left[D_{ys}\right] \left[B_{ys}\right] dy, \tag{33}$$

$$\begin{aligned} \left[M_{ys}\right]_e = \int_{A_e} \Big[ & P\left(\left[N_{u^0}\right]^T \left[N_{u^0}\right] + \left[N_w\right]^T \left[N_w\right]\right) \\ & + I_x \left(\left[N_{\theta_y}\right]^T \left[N_{\theta_y}\right]\right)\Big] dA, \end{aligned} \tag{34}$$

*2.4. Modeling the Effect of Aerodynamic Pressure and Motion Equations of the Smart Composite Plate-Stiffeners Element.* Based on the first-order theory, the aerodynamic pressure $l_h$ and moment $m_\theta$ can be described as [19, 20]

$$\begin{aligned} l_w = & \frac{1}{2}\rho_a (U\cos\alpha)^2 \\ & \cdot B\left[kH_1^* \frac{\dot{w}}{U\cos\alpha} + kH_2^* \frac{B\dot{\theta}}{U\cos\alpha} + k^2 H_3^* \theta\right] + \frac{1}{2} \\ & \cdot C_p \rho_a (U\sin\alpha)^2, \\ m_\theta = & \frac{1}{2}\rho_a (U\cos\alpha)^2 \\ & \cdot B^2\left[kA_1^* \frac{\dot{w}}{U\cos\alpha} + kA_2^* \frac{B\dot{\theta}}{U\cos\alpha} + k^2 A_3^* \theta\right], \end{aligned} \tag{35}$$

where $k = b\omega/U$ is defined as the reduced frequency, $\omega$ is the circular frequency of osscillation of the airfoil, U is the mean wind velocity, B is the half-chord length of the airfoil or half-width of the plate, $\rho_a$ is the air density, and $\alpha$ is the angle of attack.

The functions $A_i^*(K)$, $H_i^*(K)$ are defined as follows:

$$\begin{aligned} H_1^*(K) &= -\frac{\pi}{k} F(k), \\ H_2^*(K) &= -\frac{\pi}{4k}\left[1 + F(k) + \frac{2G(k)}{k}\right], \\ H_3^*(K) &= -\frac{\pi}{2k^2}\left[F(k) - \frac{kG(k)}{2}\right], \\ A_1^*(K) &= \frac{\pi}{4k} F(k), \\ A_2^*(K) &= -\frac{\pi}{16k}\left[1 - F(k) - \frac{2G(k)}{k}\right], \\ A_3^*(K) &= \frac{\pi}{8k^2}\left[\frac{k^2}{8} + F(k) - \frac{kG(k)}{2}\right], \end{aligned} \tag{36}$$

where F(k) and G(k) are defined as

$$\begin{aligned} & F(k) \\ & = \frac{0,500502k^3 + 0,512607k^2 + 0,2104k + 0,021573}{k^3 + 1,035378k^2 + 0,251293k + 0,021508}, \\ & G(k) \\ & = -\frac{0,000146k^3 + 0,122397k^2 + 0,327214k + 0,001995}{k^3 + 2,481481k^2 + 0,93453k + 0,089318}. \end{aligned} \tag{37}$$

Using finite element method, aerodynamic force vector can be described as

$$\{f\}_e^{air} = -\left[K^{air}\right]_e \{u\}_e - \left[C^{air}\right]_e \{\dot{u}\}_e + \{f\}_e^n, \tag{38}$$

where $[K^{air}]_e$, $[C^{air}]_e$ and $\{f\}_e^n$ are the aerodynamic stiffness, damping matrices, and lift force vector, respectively:

$$\left[K_e^{air}\right] = \rho_a (U\cos\alpha)^2 Bk^2 \int_{A_e} \left[ H_3^*(k) [N_w]^T [N_{\theta x}] + BA_3^*(k) \left[\frac{\partial N_{\theta y}}{\partial x}\right]^T [N_{\theta x}] \right] dA, \quad (39)$$

$$\left[C_e^{air}\right] = \rho_a (U\cos\alpha) Bk \left[ \int_{A_e} \left( H_1^*(k) [N_w]^T [N_w] + BH_2^*(k) [N_w]^T [N_{\theta x}]\, dA \right) + \int_{A_e} \left( BA_1^*(k) \left[\frac{\partial N_{\theta y}}{\partial x}\right]^T [N_w] + B^2 A_2^*(k) \left[\frac{\partial N_{\theta y}}{\partial x}\right]^T [N_{\theta x}]\, dA \right) \right], \quad (40)$$

$$\{f\}_e^n = C_p \rho_a (U\sin\alpha)^2 \int_{A_e} [N_w]^T dA, \quad (41)$$

where $A_e$ is the element area and $[N_w]$, $[N_\theta]$ are the shape functions.

From (28), (31), (32), (33), (34), and (38), the governing equations of motion of the smart composite plate-stiffeners element subjecteced to aerodynamic without damping can be derived as

$$[M^*]_e \{\ddot{u}\}_e + [C_A]_e \{\dot{u}\}_e + \left( [K^*]_e + [K_A]_e + \left[K^{air}\right]_e \right) \{u\}_e = \{f^*\}_e^m, \quad (42)$$

with $[M^*]_e = [M]_e + [M_{xs}]_e + [M_{ys}]_e$, $[K^*]_e = [K_{uu}^{ln}]_e + [K_{uu}^{nl}]_e + [K_{xs}]_e + [K_{ys}]_e$, $\{f^*\}_e^m = \{f\}_e^m + \{f\}_e^n$.

*2.5. Governing Differential Equations for Total System.* Finally, the elemental equations of motion are assembled to obtain the open-loop global equation of motion of the overall stiffened composite plate with the PZT patches as follows:

$$[M^*] \{\ddot{u}\} + \left( [C_R] + [C_A] \right) \{\dot{u}\} + \left( [K^*] + [K_A] + \left[K^{air}\right] \right) \{u\}_e = \{f^*\}^m, \quad (43)$$

where $[C_R] = \alpha[M_{uu}] + \beta([K_{uu}^{ln}] + [K_{uu}^{nl}])$, $[C_A] = -\sum_{N_{ePZT}} G_v [K_{u\phi}]_e [K_{\phi\phi}]_e^{-1} [K_{\phi\phi}]_e [K_{\phi u}^s]_e^{-1} [K_{\phi u}^s]_e$, $[K_A] = \sum_{n_{PZT}} -G_d [K_{u\phi}]_e [K_{\phi\phi}]_e^{-1} [K_{\phi\phi}]_e [K_{\phi u}^s]_e^{-1} [K_{\phi u}^s]_e$, $\alpha$ and $\beta$ are Rayleigh's coefficients, to account for inherent structural damping.

The solution of nonlinear equation (43) is carried out using Newmark direct and Newton-Raphson iteration method [11, 21].

*2.6. Numerical Applications.* A rectangle cantilever laminated composite plate is assumed to be $[0^\circ/90^\circ]_s$ with total thickness of 4mm, length of 600mm, and width of 400mm with three stiffeners along each of the directions x and y. The geometrical dimension of the stiffener is height of 5mm and width of 10mm. The material properties for plate and stiffeners made of graphite/epoxy are $E_{11}$ = 181GPa, $E_{22}$ = $E_{33}$ = 10.3GPa, $E_{12}$ = 7.17GPa, $\nu_{12}$ = 0.35, $\nu_{23}$ = $\nu_{32}$ = 0.38, are $\rho$ = 1,600kg·m$^{-3}$. Material properties for piezoelectric layer made of PZT-5A are $d_{31}$ = $d_{32}$ = -171×10$^{-12}$m/V, $d_{33}$ = 374×10$^{-12}$m/V, $d_{15}$ = $d_{24}$ = -584×10$^{-12}$m/V, $G_{12}$ = 7.17GPa, $G_{23}$ = 2.87GPa, $G_{32}$ = 7.17GPa, $\nu_{PZT}$ = 0.3, $\rho_{PZT}$ = 7,600kg·m$^{-3}$ and thickness $t_{PZT}$ = 0.15876mm, $\xi$ = 0.05, $G_v$ = 0.5, $G_d$ = 15. The effects of the excitation frequency and location of the actuators are presented through a parametric study to investigate the vibration shape of the composite plate activated by the surface bonded piezoelectric actuators. The iterative error of the load $\varepsilon_D$ = 0.02% is chosen.

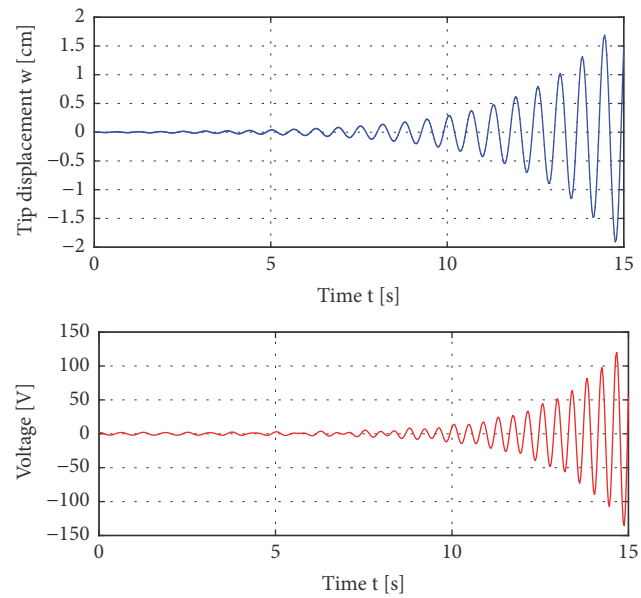


Figure 4: History of the plate at a critical airflow velocity $U_{cr}$ = 30.5m/s.

The stiffened plate is subjected to the airflow in the positive x direction as shown in Figure 1(a).

Figure 4 presents the time history response of the plate at critical airflow velocity and $\alpha = 0^\circ$.

Figure 7 shows the history of plate dynamics at $\alpha = 0^\circ$ and critical airflow velocity $U_{cr}$ = 30.5m/s. In this case, at t = 15s, tip displacement (point A in Figure 1(a)) reached 1.75cm. The plate begins to be instable and, at this time, piezoelectric voltage was 125V due to the piezoelectric effect.

## 3. Experimental Validation

*3.1. Experimental Model.* A rectangle cantilever laminated composite plate is assumed to be $[45^\circ/0^\circ/-45^\circ]_s$ with total thickness of 4mm, length of 500mm, and width of 300mm with three stiffeners along each of the directions x and y ($[45^\circ/0^\circ/-45^\circ]_s$). The geometrical dimension of the stiffener is height of 8mm and width of 10mm (Figure 5). The

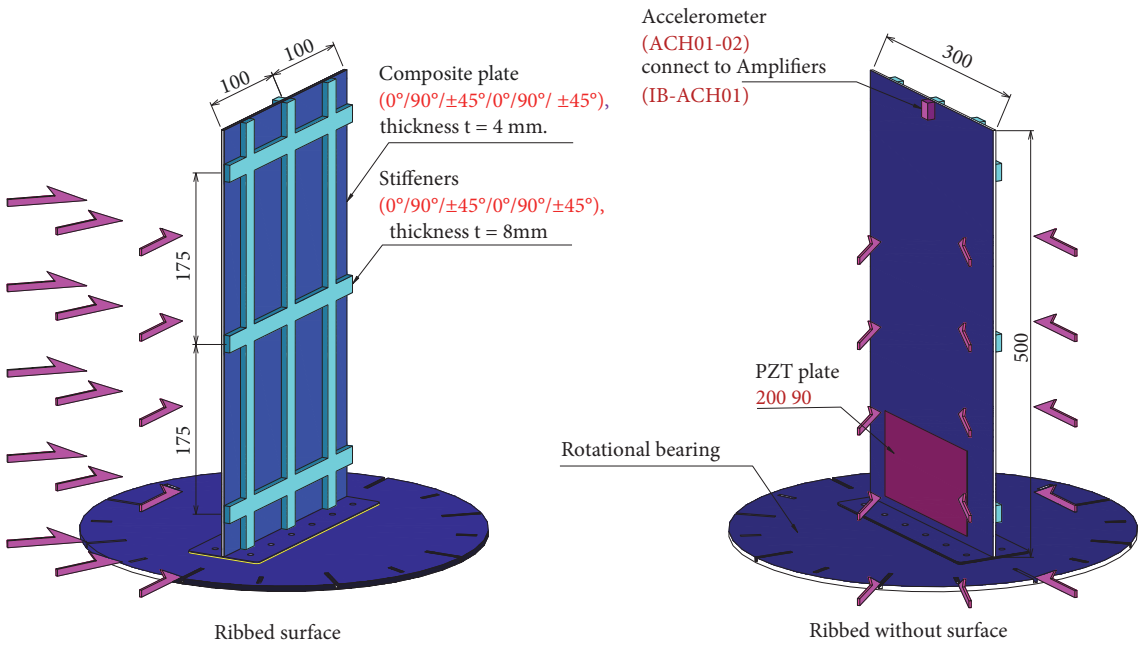


Figure 5: The preparation of experimental model.

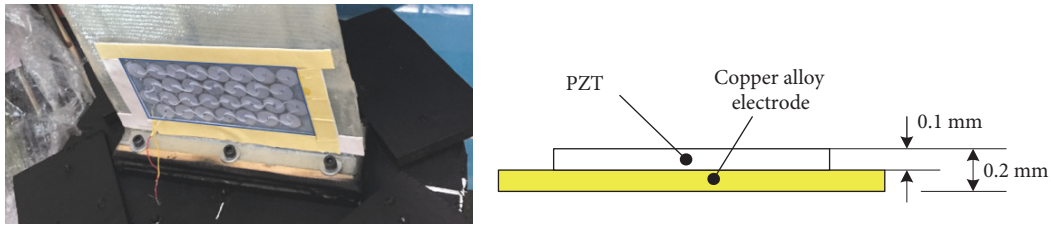


Figure 6: The real PZT model.

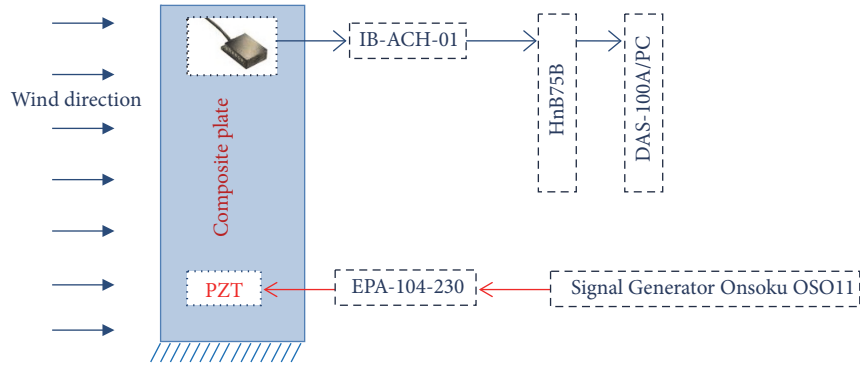


Figure 7: The diagram of experiment.

piezoelectric slice is 200 mm by 90mm dimension and placed in the location as in Figure 6. The plate and stiffeners made of T300/2500 graphite/epoxy are produced by Torayca Co., Japan. The mean values and coefficients of variation of the experimentally determined material constants are given as $E_1$ = 124.68GPa, $E_2$ = 9.6GPa, $G_{12}$ = 8.64GPa, $G_{23}$ = 2.32GPa, and $\nu_{12}$ = 0.33.

*3.2. The Diagram of Experiment.* The diagram of an experiment is shown in Figure 7. Alternating current from the electric grid running through transmitter is linearly amplified to generate voltage V with frequency $f$ imposing on PZT slice. The PZT slices attaching on the shell are playing a role to arouse the vibration of the whole system. Through two acceleration sensors attached to the shell, the dynamic

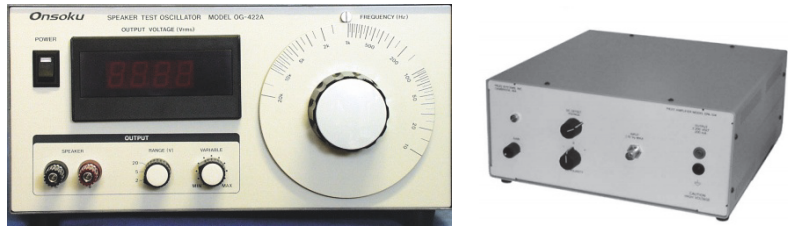


(a) The speaker test oscillator (b) The linear amplifier

Figure 8: The signal generator.

(a) (b)

Figure 9: The open wind tunnel and the bracket.

response of the shell at the location of the measurement points will be captured, displaying on the oscilloscope display and then storing in the computer.

The main experiments are shown herein:

(i) Measurement of the acceleration response of the structure at the measuring points arranged on the top of the plate corresponding to different voltage and frequency stimulation levels placed on two piezoelectric plates.

(ii) Measurement of the first free vibration of the structure.

### 3.3. Measuring Devices

*3.3.1. The Signal Generator.* The signal generator has a function to generate randomly the sinusoidal alternating current with voltage V and frequency f placing on 2 piezoelectric plates attached to the shell to establish vibration of the structure. In this experiment, the signal generator is used by combining the speaker test oscillator and a linear amplifier as in Figure 8. The speaker test oscillator is used in this experiment is Onsoku branch (Japan) model OG-422A. The specifications of the machine are as follows: the maximum output voltage: ± 200 V, the response frequency range (output): 10 ÷ 20 kHz, capacity compliant amplifier: 20 (W), compatible power supply: 100V, 115V, 220V and 240 V, frequency 50/60Hz.

*3.3.2. Generating Load Equipment.* The airflow load is created through an open wind tunnel with capacity 11kW, the area of test cross section is 1000mm×1000mm, and airflow speed can be changed from 0 to 40 m/s (Figure 9). The experimental model is placed on a bracket with a diameter $\phi$500 mm; this bracket can rotate with different angles compared to the wind direction.

*3.3.3. The Oscilloscopes.* The oscilloscope has a function which is capturing the acceleration response of the plate at the point of measurement, then displaying on screen and storing the data in the computer. The devices to measure the vibrations used in this experiment include accelerometer sensor (2 sensors), two piezoelectric data receivers HnB75B, oscilloscope display Tektronix TDS-1012, and a computer. The accelerometer sensors used in this experiment are type ACH01-02 (Figure 9(a)). The specifications of these accelerometer sensors include parameters: the sensitivity 10mV/g, frequency band 1,0Hz ÷ 20kHz, dynamic range: ± 250g, resolution $40\mu g\sqrt{\text{Hz}}$, resonant frequency: > 35kHz, linearity: 0.1%, and the maximum pick: 1000g (g: gravity acceleration).

Two piezoelectric channels' data acquisition HnB75B has a function to amplify the electrical signals from the sensor to the oscilloscope and the computer (Figure 9(b)). The specifications of this device include: number of channels - 2 simultaneous channels, voltage range measurement: 0 ÷ 5V, accuracy: +/- 0.2%, sampling frequency: maximum 10 kHz, connection port: 1 com port, 2 AC ports.

Through the simulation program set up already in devices and computer, the vibrations of the plate at measurement points are displayed on the screen of Tektronix TDS-1012 machine with the vibration parameters at each oscillation cycle (Figure 10(c)).

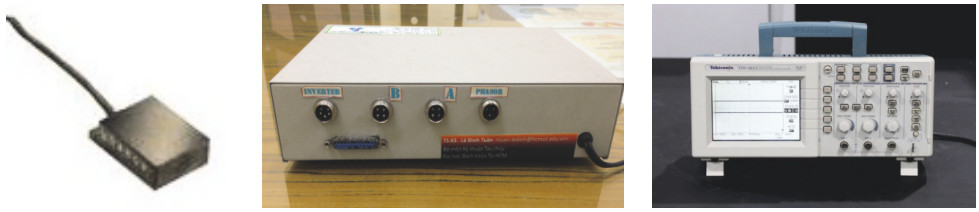

(a) The acceleration sensor (b) HnB75B data receiver (c) The oscilloscope display

Figure 10: The oscilloscopes.

Table 1: The maximum acceleration at U = 5m/s.

| Method | $a^{max}$ [m/s$^2$] | $\alpha$[deg] | Error [%] |
|---|---|---|---|
| Experiment | 0.050 | 45 | 11.8 |
| FEM | 0.0559 | | |
| Experiment | 0.061 | 22.5 | 10.7 |
| FEM | 0.0675 | | |
| Experiment | 0.072 | 0 | 10.1 |
| FEM | 0.0793 | | |

**Comment**: The theoretical and experimental results for the acceleration response of the plate at the point of measurement over time are fairly uniform, with maximum error of 11.80% for acceleration being acceptable. Thus, the results of the experiment showed the relevance of algorithms and programs in published theoretical research.

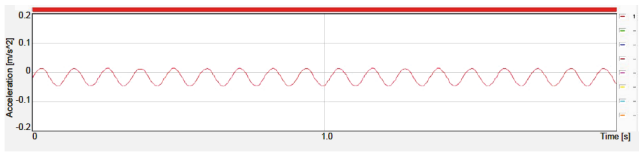

Figure 11: The acceleration response in one measurement with $\alpha$ = 0°, U = 5m/s.

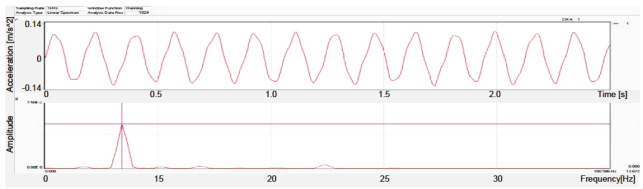

Figure 12: The acceleration response and frequency spectrum with f = 13.672Hz, U = 10m/s, $\alpha$ = 45°.

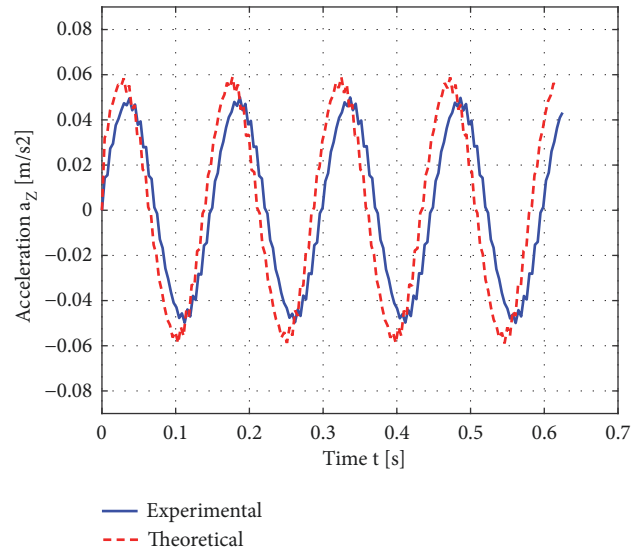


Figure 13: The acceleration response of plate at the measuring position (U = 5m/s).

*3.4. The Results of Measuring Acceleration Response Experiment.* In this experiment, the authors conduct three cases: $\alpha$ = 0°, $\alpha$ = 22.5°, and $\alpha$ = 45°.

**For $\alpha$ = 0°:** The speed of the airflow U = 5m/s and 10 m/s; the voltage $V_{in}$ = 9.30V, and $K_{amp}$ = 20. Hence the voltage level will be $V_{in} \times K_{amp}$ = 9.30 V × 20 = 186.0V; sampling frequency $f_{samp}$ = 1000 Hz; frequency of stimulation $f$ = 6.944 Hz.

**For $\alpha$ = 22.5°:** The speed of the airflow U = 5m/s and 10m/s; the voltage $V_{in}$ = 9.50V, and $K_{amp}$ = 20. Hence the voltage level will be $V_{in} \times K_{amp}$ = 9.50 V × 20 = 190.0V; sampling frequency $f_{samp}$ = 1000 Hz; frequency of stimulation $f$ = 6.981 Hz.

**For $\alpha$ = 45°:** The speed of the airflow U = 5m/s and 10m/s; the voltage $V_{in}$ = 9.20V, and $K_{amp}$ = 20. Hence the voltage level will be $V_{in} \times K_{amp}$ = 9.20 V × 20 = 184.0 V; sampling frequency $f_{samp}$ = 1000 Hz; frequency of stimulation f = 6.993 Hz.

The acceleration-time and amplitude-frequency response at the measuring point of the above stiffened composite plate with PZT patches are shown in Figures 11 and 12.

We calculate the acceleration response for the above stiffened composite plate with PZT patches by our computer program. The acceleration response at the measuring point of the plate will be compared with those of experimental ones and is given in Figure 13 and Table 1.

## 4. Conclusion

The nonlinear dynamics analysis of the piezoelectric stiffened composite plate subjected to airflow using the finite element and experimental method has been presented. In this paper, we have presented a nine-noded stiffened rectangular composite plate element with PZT patches for the nonlinear vibration analysis of the piezoelectric stiffened composite plates subjected to airflow. The critical velocity of the airflow is determined by numerical calculations. The finite element results compare well with experimental ones. It is recommended that the present formulation can be used to determine the characteristics of the vibration and stability in the analysis and design of the piezoelectric stiffened composite plate structures subjected to airflow applied to the flying instruments.

## Data Availability

The data used to support the findings of this study are available from the corresponding author upon request.

## Conflicts of Interest

The authors declare that they have no conflicts of interest.

## References

[1] J. F. Haskins and J. L. Walsh, "Vibrations of ferroelectric cylindrical shells with transverse isotropy. I. Radially polarized case," *The Journal of the Acoustical Society of America*, vol. 29, pp. 729–734, 1957.

[2] R. A. Toupin, "Piezoelectric relations and the radial deformation of a polarized spherical shell," *The Journal of the Acoustical Society of America*, vol. 31, pp. 315–318, 1959.

[3] H. F. Tiersten, *Linear Piezoelectric Plate Vibrations*, Springer US, Boston, MA, 1969.

[4] N. T. Adelman and Y. Stavsky, "Vibrations of radially polarized composite piezoceramic cylinders and disks," *Journal of Sound and Vibration*, vol. 43, no. 1, pp. 37–44, 1975.

[5] V. Balamurugan and S. Narayanon, "Active Vibration Control of Smart Stiffened Plates using Distributed Piezoelectric Sensors and Actuators," *Forum Acusticum*, pp. 41–46, 2005.

[6] R. L. Wankhade and K. M. Bajoria, "Shape Control and Vibration Analysis of Pi-ezolaminated Plates Subjected to Electro-Mechanical Loading," *Open Journal of Civil Engineering*, vol. 06, no. 03, pp. 335–345, 2016.

[7] P. veera Sanjeeva Kumar and B. Chandra Mohana Reddy, "Vibration Analysis of Smart Composite Laminate Plates using Higher Order Theory," *International Journal of Mechanical And Production Engineering*, vol. 5, no. 2, pp. 66–69, 2017.

[8] B. Sangamesh, Sai. Herakal Kumar Dathrika, P. Giriraj Goud, and P. Sravan, "Finite Element Analysis of Smart Composite Plate under Thermal Environment , AIJRRLJSM, Volume 1, Issue 5, 2016," *May*, pp. 105–109, 2016.

[9] K. Makihara, J. Onoda, and K. Minesugi, "Flutter Suppression of Cantilevered Plate Wing using Piezoelectric Materials," *International Journal of Aeronautical and Space Sciences*, vol. 7, no. 2, pp. 70–85, 2006.

[10] K. Zafer and M. Zahit, "Flutter Analysis of a Laminated Composite Plate with Temperature Dependent Material Properties," pp. 106–114, 2016.

[11] N. T. Chung, H. X. Luong, and N. T. Xuan, "Dynamic stability analysis of laminated composite plates with piezoelectric layers," *Vietnam Journal of Mechanics*, vol. 36, no. 2, pp. 95–107, 2014.

[12] N. N. Thuy and N. T. Chung, "Dynamic Analysis of Smart Stiffened Composite Plates using Higher Order Theory," in *Proceedings of the In Proceedings of the National Conference on Mechanics 10th, Vietnam 12-2017*, pp. 1197–1204, 2017.

[13] J. Yang, *The Mechanics of Piezoelectric Structures*, World Scientific Publishing Co. Pte. Ltd., 2006.

[14] J. N. Reddy, "Mechanics of laminated composite plates and shells," in *Theory and Analysis*, CRC Press, 2nd edition, 2004.

[15] K. J. Bathe and E. L. Wilson, "Numerical Method in Finite Method Analysis , Prentice Hall of India Private Limited," *Numerical Method in Finite Method Analysis , Prentice Hall of India Private Limited*, 1978.

[16] T. I. Thinh and L. K. Ngoc, "Static and dynamic analysis of laminated composite plates with integrated piezoelectrics," *Vietnam Journal of Mechanics*, vol. 30, no. 1, pp. 55–66, 2008.

[17] L. Meirovitch, *Methods of analytical dynamics*, Dover Publications, Inc., Mineola, NY, 2003.

[18] B. Patnaik, G. Heppler, and W. Wilson, "Sensor effectiveness coefficients for piezoelectric materials," in *Proceedings of the 1995 American Control Conference - ACC'95*, pp. 3801-3802, Seattle, WA, USA.

[19] J. Holmes, *Wind Loading of Structures, Third Edition*, CRC Press, 2015.

[20] R. H. Scanlan and N. P. Jones, "Aeroelastic Analysis of Cable-Stayed Bridges," *Journal of Structural Engineering*, vol. 116, no. 2, pp. 279–297, 1990.

[21] C. R. Farrar, J. L. Beck, and A. K. Chopra, "Earthquake engineering applications of structural health monitoring," *Earthquake Engineering & Structural Dynamics*, vol. 42, no. 9, pp. 1413-1414, 2013.